

Probing Boundary Spins in the Su-Schrieffer-Heeger-Hubbard model

Armando A. Aligia,^{1,*} Alejandro M. Lobos,^{2,3,†} Lucila Peralta Gavensky,^{4,5} and Claudio J. Gazza⁶

¹*Instituto de Nanociencia y Nanotecnología CNEA-CONICET, GAIDI,
Centro Atómico Bariloche and Instituto Balseiro, 8400 Bariloche, Argentina*

²*Instituto Interdisciplinario de Ciencias Básicas - Consejo Nacional de Investigaciones Científicas y Técnicas*

³*Facultad de Ciencias Exactas y Naturales - Universidad Nacional de Cuyo*

⁴*Center for Nonlinear Phenomena and Complex Systems,
Université Libre de Bruxelles, CP 231, Campus Plaine, B-1050 Brussels, Belgium*

⁵*International Solvay Institutes, 1050 Brussels, Belgium*

⁶*Instituto de Física Rosario, CONICET, and Facultad de Ciencias Exactas, Ingeniería y Agrimensura,
Universidad Nacional de Rosario, 2000 Rosario Argentina*

Studying boundary excitations provides a powerful approach to probe correlations in topological phases. We propose that localized spins near the ends of a Su–Schrieffer–Heeger–Hubbard chain embedded in an insulating environment can be detected experimentally using scanning tunneling microscopy (STM) combined with electron spin resonance (ESR). When the STM tip is in the contact regime, the tip–end-spin coupling realizes an effective Anderson impurity problem, giving rise to a Kondo peak at low bias. Spatially resolving the Kondo resonance width as the STM tip approaches the chain ends provides an indirect yet clear signature of these localized spins. To support this proposal, we use density-matrix renormalization group (DMRG) to calculate the spin gap and spin projection of end states for chains of various lengths and interaction strengths U at half-filling. In the non-interacting limit ($U = 0$), we derive simple analytical expressions that reproduce the numerical results for sufficiently long chains. We also discuss how the correlated phase of the isolated chain is characterized by boundary zeros in its single-particle Green’s function, and briefly comment on their localization properties in relation to the boundary spins.

I. INTRODUCTION

Non-interacting topological insulators are at present well understood. They can be characterized by a non-vanishing topological invariant [1]. In particular for the Su-Schrieffer-Heeger chain (SSH) [2], the Zak Berry phase [3] acts as a \mathbb{Z}_2 number which distinguishes the topological and non-topological phases [4]. For an open non-interacting SSH, the topological phase has one eigenstate of zero energy for each spin, localized at each end of the chain, which imply poles at zero energy in the Green’s function.

In the interacting case, the states at zero energy disappear, however the Berry phase or similar topological invariants [5] continue to separate topological and non-topological phases. In particular, an invariant based on the Green’s function at zero energy has been proposed [6, 7]. Several numerical studies have shown that the boundary poles of the non-interacting Green’s function are transformed into zeros when correlations are included in the topological phase [7–9]. It has been argued that these zeros reflect the presence of in-gap spin excitations (spinons) at zero energy [8, 9]. The appearance of zeros in the Green’s functions is responsible for a topological transition in a two-channel spin-1 Kondo model with easy-plane anisotropy which explains several relevant experiments for magnetic molecules on metallic substrates [10–13]. The importance of these zeros has also been

stressed in different contexts [14–19] and particularly in relation with the spinons [9, 16, 17]. In the case of a SSHC with open boundary conditions in the topological phase, it has been established that localized spins remain at the ends in the presence of interactions [7], but the relation between the localization length of these spin modes and that of the boundary zeros of the single-particle Green’s function has not been addressed. Moreover, the evolution of these localized states (in particular, their magnitude and spatial extent) from the non-interacting to the strongly-interacting limit as a function of the interaction parameter has not, to our knowledge, been thoroughly investigated. Exploring these aspects would be of considerable interest.

From the experimental perspective, the detection of localized spins at the ends of interacting spin chains has attracted a lot of attention lately. In recent scanning tunneling microscopy (STM) experiments, the Kondo resonance at zero bias has been used to identify localized spins at the ends of topological chains deposited on metallic surfaces [20–22]. In these works, the intensity of the atomically-resolved Kondo resonance has been used to map the spin profile of the topological end states. However, for potential applications where a metallic environment is not desirable (e.g., spin qubits requiring long quantum coherence times T_2) the Kondo resonance becomes unobservable and other detection tools are necessary. The recent advent of electron spin resonance combined with STM (ESR-STM) has enabled to extract locally-resolved dynamic information of such isolated spin systems, and has been successfully applied in spin-1/2 Ti clusters deposited on an insulating MgO de-

* aaligia@gmail.com

† alejandro.martin.lobos@gmail.com

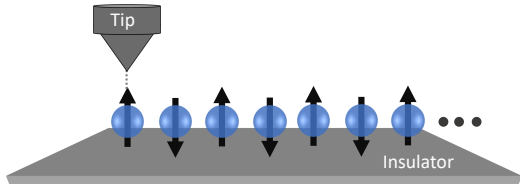


FIG. 1. (Color online) Scheme of an interacting spin chain on top of an insulating surface. In the contact regime, the conduction electrons in the STM tip can directly hybridize with the underlying localized spin states, effectively screening them.

coupling layer [23]. However, while this technique enables the detection of localized end states in topological spin chains in non-metallic environments, it has been pointed out that its spectral resolution would be severely restricted in the case of long chains ($L > 30$ atoms) [24]. Therefore, complementary methods would be highly desirable.

In this article we theoretically investigate how STM in the contact regime, possibly combined with ESR, can provide critical insights into the localized spin degrees of freedom of this correlated insulator (see Fig. 1), thereby offering complementary information to standard STM-ESR spectroscopy. In fact it is known that magnetic molecules on substrates can enter the contact regime when the STM tip is sufficiently near to the molecule, favoring a direct hybridization between the conduction electrons of the tip and the localized electrons of the molecule. Examples are experiments with nickelocene molecules on metallic surfaces [25–27] and the corresponding theory [11], and a Co atom on a Cu(100) surface [28].

Therefore, as explained in Section IV, when the STM tip approaches an end of a SSHC in its topological phase, the problem can be mapped into an effective impurity Anderson model, and from the width (instead of the intensity) of the measured Kondo resonance, the magnitude and degree of localization of the spin can be inferred. To that end, we propose an effective Hamiltonian for the interaction of the low-energy states of an interacting finite topological SSHC with an STM tip. Using the density-matrix renormalization group (DMRG), we compute the spin gap and the expectation value of the spin projection of several chains for different values of U , which serve as an input for the effective tip-system Hamiltonian. Additionally, for a short SSHC, the spins at the ends interact leading to a finite energy splitting, which can be detected by STM-ESR [24, 29–31]. For long chains naturally an applied magnetic field also leads to a measurable splitting. Recently both a Kondo resonance and ESR have been observed for an organic molecule coupled to a metallic surface [32], and ESR was used to study

spin fractionalization in a Haldane system [33].

The paper is organized as follows. Section II describes the SSHC model. Section III presents a simple analytical solution for the end states of a non-interacting topological, open SSHC, starting from the exact zero-energy eigenstates of the infinite chain. Section IV introduces the effective Hamiltonian relevant for the ESR-STM experiments. Section V contains the numerical DMRG results. Section VI discusses the emergence of zero eigenvalues of the zero-frequency single-particle Green’s function and their localization properties. Finally, Section VII provides a summary and discussion.

II. THEORETICAL MODEL

The SSHC was originally proposed to describe the physics of polyacetylene, where alternating strong and weak bonds between carbon atoms lead to a dimerized lattice [2]. More recently, the interest in the system raised due to its topological properties [4]. Two distinct topological states are separated by a \mathbb{Z}_2 number [4, 5] that changes if the strong bonds are the even or the odd ones. The topological phase corresponds to the case when the first bond of the chain is weak, and in this case (as we show in detail in the next Section) the model has eigenstates of zero energy localized at the ends of the chain.

In the interacting SSHC, the zero-energy states disappear, but the topological properties of the model remain [5, 7] and spin excitations localized at the ends persist in the topological phase. In particular, in the strong-coupling limit, the model is equivalent to a spin-1/2 alternating XXZ model [34, 35], and spin-1/2 edge excitations have been detected in an experimental realization of this model using graphene nanoribbons [21].

The Hamiltonian of the electron-hole symmetric interacting open SSHC, representing an atomic chain deposited on top of an insulating surface (see Fig. 1), can be written in compact form as

$$\hat{H} = \sum_{j=1}^{L-1} -[t_0 + \delta(-1)^j] \sum_{\sigma=\uparrow,\downarrow} \left(\hat{c}_{j+1\sigma}^\dagger \hat{c}_{j\sigma} + \text{H.c.} \right) + U \sum_{j=1}^L \left(\hat{n}_{j\uparrow} \hat{n}_{j\downarrow} - \frac{1}{2} \sum_{\sigma=\uparrow,\downarrow} \hat{n}_{j\sigma} \right), \quad (1)$$

where $\hat{c}_{j\sigma}^\dagger$ creates an electron with spin σ at site j and $\hat{n}_{j\sigma} = \hat{c}_{j\sigma}^\dagger \hat{c}_{j\sigma}$ is the electron number operator. Unless otherwise stated, we assume that the number of sites L is even and the system consists of $L/2$ unit cells. In the following we denote by t_1 (t_2) the hopping of the odd (even) bonds:

$$t_1 = t_0 - \delta, \quad t_2 = t_0 + \delta, \quad (2)$$

which, without loss of generality, can be assumed positive (i.e., changing if necessary the phases of the $c_{j\sigma}$ via

a gauge transformation). The topological phase corresponds to the case $t_1 < t_2$ [4, 5, 7].

III. STATES NEAR ZERO ENERGY FOR $U = 0$

In the non-interacting case, the eigenstates of vanishing energy can be easily found with the method of Alase *et al.* [36–38]. This result sheds light of what is expected in the general case. The method is particularly suitable to provide analytical results when the energy is known (for example zero energy) because self-consistent equations can be avoided [38]. In the topological phase of the non-interacting open SSCH for $L \rightarrow \infty$, localized states with zero energy are present at each end. Since it is easy to verify that these states are zero-energy states, we just write the result we obtained for the states localized at the left ($|L\sigma\rangle$) and the right ($|R\sigma\rangle$) of the infinite chain with spin σ . We can define these states as

$$|L\sigma\rangle = \hat{l}_\sigma^\dagger |0\rangle, \quad (3)$$

$$|R\sigma\rangle = \hat{r}_\sigma^\dagger |0\rangle, \quad (4)$$

where the second-quantized operators \hat{l}_σ^\dagger and \hat{r}_σ^\dagger are defined as

$$\hat{l}_\sigma^\dagger = \sqrt{\frac{1-z^2}{1-z^L}} \sum_{j=1}^{L/2} z^{j-1} \hat{c}_{2j-1\sigma}^\dagger, \quad (5)$$

$$\hat{r}_\sigma^\dagger = \sqrt{\frac{1-z^2}{1-z^L}} \sum_{j=1}^{L/2} z^{L/2-j} \hat{c}_{2j\sigma}^\dagger, \quad (6)$$

$$z = -t_1/t_2, \quad (7)$$

where for later use we have generalized the definitions of the normalized states to chains of finite-length L . Note that for $|L\sigma\rangle$ only odd sites enter in the sum with decreasing amplitude z in such a way that $H|L\sigma\rangle = 0$. Similarly only even sites enter $|R\sigma\rangle$. In fact the inversion symmetry I centered at the midpoint between sites $L/2$ and $L/2 + 1$, which interchanges sites j and $L - j + 1$ ($\hat{c}_{j\sigma}^\dagger \leftrightarrow \hat{c}_{L-j+1\sigma}^\dagger$) is a symmetry of the Hamiltonian ($[H, I] = 0$) and $|R\sigma\rangle = I|L\sigma\rangle$.

For a finite chain, although the method of Alase *et al.* can be applied [38], we follow a simpler approach and start from Eqs. (3) and (4) as approximate eigenstates. After some algebra we obtain

$$\begin{aligned} H|L\sigma\rangle &= -t_{LR}|R\sigma\rangle + t_c|A\sigma\rangle, \\ H|R\sigma\rangle &= -t_{LR}|L\sigma\rangle + t_c|B\sigma\rangle, \\ t_{LR} &= \frac{1-z^2}{1-z^L} z^{L/2-1} t_1, \end{aligned} \quad (8)$$

where all states are orthonormal, and states $|A\sigma\rangle$ and $|B\sigma\rangle$ are states in the continuum with energy above the

gap, given by

$$\begin{aligned} t_c|A\sigma\rangle &= \sqrt{\frac{1-z^2}{(1-z^L)^3}} z^{L/2-1} t_1 [(1-z^2) \sum_{j=1}^{L/2-1} z^{L/2-j} \hat{c}_{2j\sigma}^\dagger \\ &\quad + (z^L - z^2) \hat{c}_{L\sigma}^\dagger] |0\rangle, \\ |B\sigma\rangle &= I|A\sigma\rangle. \end{aligned} \quad (9)$$

As shown below, already for a chain of moderate length such that $z^{L/2} \ll 1$, the terms proportional to t_c [given by Eqs. (9)] can be neglected and the eigenstates and energies are

$$\begin{aligned} |S\sigma\rangle &= (|L\sigma\rangle + |R\sigma\rangle)/\sqrt{2}, E_S = -t_{LR} \\ |D\sigma\rangle &= (|L\sigma\rangle - |R\sigma\rangle)/\sqrt{2}, E_D = t_{LR} \end{aligned} \quad (10)$$

The many-body ground state is a singlet with the states $|S\sigma\rangle$ occupied for both spins. The lowest triplet state has one electron occupying a $|S\sigma\rangle$ and the other a $|D\sigma\rangle$ state. In particular for total spin projection $S_z = 1$ the state is simply $\hat{l}_\uparrow^\dagger \hat{r}_\uparrow^\dagger |0\rangle$. Therefore the spin gap is

$$\Delta_s = 2t_{LR} = 2 \frac{1-z^2}{1-z^L} z^{L/2-1} t_1. \quad (11)$$

This energy can be measured by the ESR-STM technique [23, 33].

Regarding the terms proportional to t_c in Eq. (8), note that from the norm of $t_c|A\sigma\rangle$, and neglecting z^L compared to 1, one has

$$t_c^2 \simeq z^L (1-z^2) t_1^2. \quad (12)$$

The eigenstates near zero energy are separated from the rest of the spectrum by an energy $E = t_2 - t_1$ (half the gap of the periodic non-interacting SSHC [4]). Therefore, from second-order perturbation theory, the correction of the energies of the low-energy eigenstates due to the states $|A\sigma\rangle$ and $|B\sigma\rangle$ is of order $t_c^2/E = z^{L+2}(t_1 + t_2)$ and the relative error in the spin gap is of order

$$t_c^2/(E\Delta_s) \simeq z^{L/2+1} t_1/(t_2 - t_1) \simeq z^{L/2+2}/(1+z). \quad (13)$$

Since we are assuming $z^L \ll 1$, we conclude that the terms proportional to t_c can be safely neglected.

IV. EFFECTIVE HAMILTONIAN FOR THE ESR-STM

As schematically shown in Fig. 1, we now assume that the STM tip approaches one end of an open long SSHC, and we assume the tip is in the contact regime [11, 26, 28]. Under such conditions, the localized end states can jump to the tip giving rise to a resonant level model. Choosing

for simplicity the left end, the Hamiltonian of the tip coupled to the spin-chain takes the form

$$\hat{H}_1(j) = \sum_{k\sigma} [\varepsilon_{k\sigma} \hat{t}_{k\sigma}^\dagger \hat{t}_{k\sigma} + V_j (\hat{l}_\sigma^\dagger \hat{t}_{k\sigma} + \text{H.c.})], \quad (14)$$

where the first term describes a continuum of states of the STM tip giving rise to a featureless local density of states, and the second term corresponds to the hybridization with the left end-state at site j . The value of V_j depends on the position of the tip along the chain which, due to its atomic resolution, is proportional to the coefficient of $\hat{c}_{j\sigma}^\dagger$ in Eq. (5). For example, for a long non-interacting chain it is $\sqrt{1-z^2}V$ for $j=1$, 0 for $j=2$, $z^2\sqrt{1-z^2}V$ for $j=3$, etc., with V a constant that depends on the distance between the STM tip and the sample. The tip-chain coupling can be modeled by

$$V_j = \sqrt{2|\langle \hat{S}_j^z \rangle|} V, \quad (15)$$

where \hat{S}_j^z is the spin projection at site j , and where the expectation value is taken in the lowest energy many-body state with total spin projection $S_z = 1$, i.e., the state $\hat{l}_\uparrow^\dagger \hat{r}_\uparrow^\dagger |0\rangle$. While Eq. (15) is analytically exact only in the non-interacting case and merely an educated guess for the interacting one, the numerical results presented in Section V show (see Fig. 4) that it remains a remarkably accurate approximation in the latter.

The above model corresponds to an effective Anderson model, in which a localized state with spin 1/2 (in our case the spin degenerate ground state of a semi-infinite SSHC in its topological phase) is hybridized with a conduction band (the metallic states of the STM tip). The spectral density of the localized states in the non-interacting case is well known and consists of a peak centered at the Fermi level, with the special feature of having a spatially-dependent width $\Gamma_j = \rho V_j^2$, where ρ is the spectral density per spin of the tip, assumed independent of energy. In contrast, the density of states of the conduction electrons has a dip of the same magnitude Γ_j .

In the interacting case $U \neq 0$, the localized spin remains at the end. The situation is particularly simple for $t_1 = 0$. In this case, $\hat{c}_{1\sigma}^\dagger |0\rangle$ are eigenstates of the isolated first site of the chain, with energy $-U/2$. Including the hybridization with the tip, because of the electron-hole symmetry of our SSHC [Eq. 1], the model takes the form of the symmetric impurity-Anderson model (SIAM).

In the general interacting case of an infinite chain, there exist two degenerate states with total spin projection $S_z = \pm 1/2$, localized at the left end of the chain but extending beyond the first site. These states can be mapped onto the corresponding states of the SIAM (or Kondo model for large U), and these two states can be flipped via second-order hopping to the STM tip. The spin-flip terms are the primary source of the renormalization group flow to strong coupling in the Kondo model [39]. Therefore we expect that the following SIAM is valid in the general case

$$\hat{H}_2(j) = \hat{H}_1(j) + U \left(\hat{n}_{L\uparrow} \hat{n}_{L\downarrow} - \frac{1}{2} \sum_{\sigma=\uparrow,\downarrow} \hat{n}_{L\sigma} \right), \quad (16)$$

where $\hat{n}_{L\sigma} = \hat{l}_\sigma^\dagger \hat{l}_\sigma$ for either $U = 0$ or $t_1 \rightarrow 0$, and the effective occupancy of the corresponding end state in the general case.

The localized spectral density of the model Eq. (16) is well known. In the Kondo regime at low energies it consists of a peak whose half width is of the order of the Kondo temperature T_K . Using the Haldane formula [40]

$$T_K(j) \simeq \sqrt{\frac{U\Gamma_j}{2}} \exp\left(\frac{-8\pi U}{\Gamma_j}\right). \quad (17)$$

Instead, the spectral density of the conduction electrons has a dip of the same magnitude. In STM experiments in the contact regime a peak corresponding to the spectral density of localized electrons has been measured [26, 28], as expected for the SSHC on an insulating film. However, one might also have a dip arising from conduction electrons or an asymmetric line shape caused by Fano interference [41]. In some cases, even extended atomic orbitals play the dominant role [42]. However, in all these cases there is a feature at the Fermi level whose characteristic energy is easy to identify experimentally and is given by T_K . Assuming the parameters U and V do not vary along the chain, the local variation of $T_K(j)$ from one site to the other would permit to extract the profile of $\langle \hat{S}_j^z \rangle$ via Eq. (15).

To calculate V_j in the general interacting case, we proceed as follows. In the Kondo problem, it is known that the relevant hybridization processes are those which lead to a spin flip between localized spin states $|\uparrow\rangle$ and $|\downarrow\rangle$ (along with an inverted spin flip in the conduction band) in second order [39]. Then, our general strategy is to extract the effective hybridization in the interacting case from the relation $(V_j/V)^2 = \left| \langle \downarrow | c_{j\downarrow}^\dagger c_{j\uparrow} | \uparrow \rangle \right|^2$, obtained from a Schrieffer-Wolff transformation [43] neglecting the energy dependence of the intermediate states. For a semi-infinite chain, the ground state with spin up can be written as

$$|\uparrow\rangle = a_0 |1/2\rangle + a_{1\uparrow} c_{j\uparrow}^\dagger |0\rangle + a_{1\downarrow} c_{j\downarrow}^\dagger |1\rangle + a_2 c_{j\uparrow}^\dagger c_{j\downarrow}^\dagger |1/2, \beta\rangle, \quad (18)$$

where the states $|S_z, \gamma\rangle$ above are many-body states of the system in the absence of the site j , and are classified by their total spin projection S_z and, when necessary, by an additional index γ to distinguish states with the same S_z . Without loss of generality, the coefficients a_ν can be assumed real. The ground state with spin down is the time reversal of the state above

$$|\downarrow\rangle = a_0 | -1/2\rangle + a_{1\uparrow} c_{j\downarrow}^\dagger |0, \beta\rangle - a_{1\downarrow} c_{j\uparrow}^\dagger | -1\rangle + a_2 c_{j\uparrow}^\dagger c_{j\downarrow}^\dagger | -1/2, \beta\rangle, \quad (19)$$

where each state $|S_z, \gamma\rangle$ here is the time reversal of the corresponding one in Eq. (18). Note that all of them are orthogonal to the previous ones because of the different S_z except $|0, \beta\rangle$ and $|0\rangle$. Then

$$(V_j/V)^2 = |\langle \downarrow | c_{j\downarrow}^\dagger c_{j\uparrow} | \uparrow \rangle| = a_{1\uparrow}^2 |\langle 0, \beta | 0 \rangle|. \quad (20)$$

In the case of sufficiently long but finite chain of length L , a practical way to calculate V_j is to take into account that by inversion symmetry, the site j can be mapped onto the site $L + 1 - j$ and vice versa and that the state with $S_z = 1$ (-1) can be constructed from $|\uparrow\rangle$ ($|\downarrow\rangle$) at both ends. Then, the effective hopping is computed as

$$(V_j/V)^2 = |\langle -1 | c_{j\downarrow}^\dagger c_{L+1-j\downarrow}^\dagger c_{L+1-j\uparrow} c_{j\uparrow} | 1 \rangle|^2. \quad (21)$$

Eq. (21) is valid for all sites where either the left or right spin end state dominates, but it becomes inaccurate for a few sites near the center of the chain, where both end states have comparable weight.

Finally for a finite chain, there is an effective interaction between the spins at both ends which is responsible for the spin gap. In this case, the total effective Hamiltonian has the form

$$\hat{H}_{\text{eff}} = \hat{H}_2 + \Delta_s \hat{\mathbf{S}}_L \cdot \hat{\mathbf{S}}_R, \quad (22)$$

where $\hat{\mathbf{S}}_L$ and $\hat{\mathbf{S}}_R$ are the spin operators of both ends. The essential physics of this model is known from previous studies of similar systems [44–50]. If $T_K \gg \Delta_s$, with T_K given by Eq. (17), the spectral density of the localized states at zero temperature $T = 0$ consist of a peak of half width T_K but with a very narrow dip at the Fermi energy of width $T_0 \sim T_K \exp(-\pi T_K / \Delta_s)$ [44, 50]. For $T > T_0$ this dip disappears. Instead if $T_K \ll \Delta_s$, the spectrum consists of two peaks at energies near $\pm \Delta_s / 2$. However, in this regime we expect the ESR-STM technique to describe more accurately the excitation energy Δ_s . For $T_K \sim \Delta_s$, the spectral density consists of two peaks with a dip in between at the Fermi energy but without a simple quantitative description.

In any case, the effective T_K can be tuned by moving the STM tip vertically with respect to the chain. As the tip approaches the chain, the hybridization V , and therefore Γ_j , increase. Because V changes exponentially with tip-sample distance [51], and T_K itself depends exponentially on V , it is experimentally straightforward to access the aforementioned limiting regimes, in which either the width of the main spectral feature as a function of position, or the energy of the ESR signal give direct information on the topological state.

V. NUMERICAL RESULTS

In this section, we show numerical results for the SSHC (without including the STM tip) which illustrate our

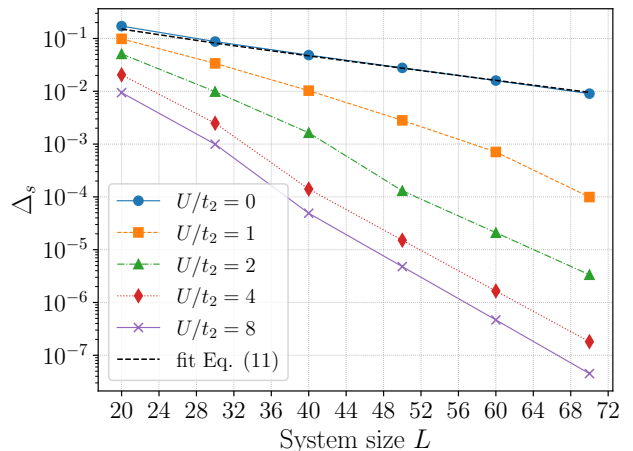


FIG. 2. (Color online) Spin gap as a function of system size for $t_1 = 0.9$ and several values of U . The dashed line for $U = 0$ corresponds to Eq. (11). Dataset available in Ref. [52].

proposal. To that end, using the DMRG method implemented through the ITENSOR library [53], we have computed the spin gap Δ_s and the spin profile of the localized spin \hat{S}_j^z taken in the lowest-energy state with total spin projection $S_z = 1$, of interacting play with different lengths L and for different values of U . These are the quantities which permit to predict the STM differential conductance and the ESR-STM signal according to the previous Section. All calculations were carried out with a maximum bond dimension sufficient to ensure that the truncation error remained below 10^{-9} . This assures that errors of the DMRG computation are smaller than symbol sizes in each figure. In what follows we take $t_2 = 1$ as the unit of energy.

In Fig. 2 we show the resulting spin gap, computed as $\Delta_s = E_g^{(1)} - E_g^{(0)}$, where $E_g^{(S)}$ is the ground-state energy in the spin- S subspace, for several lengths of the chain and different values of the interaction U . In the non-interacting case, $U = 0$, the numerical results are in excellent agreement with the analytical expression given by Eq. (11), particularly for long chains. There is an exponential decay with system size. For larger values of U the dependence on the length of the chain continues to be approximately exponential, but the decay is faster and the gap is smaller. Increasing U from 0 to 8, the spin gap Δ_s decreases by slightly more than an order of magnitude for $L = 20$, but by more than five orders of magnitude for $L = 70$. As it was discussed before for spin-1 chains [24] a very small excitation energy cannot be detected by STM-ESR, unless a Zeeman splitting is induced by an applied magnetic field. This is precisely the regime (i.e., the case of long chains and large U) where our proposed method would be most useful and would complement the standard STM-ESR technique.

In Fig. 3(a) the expectation values $\langle \hat{S}_j^z \rangle$ as a function

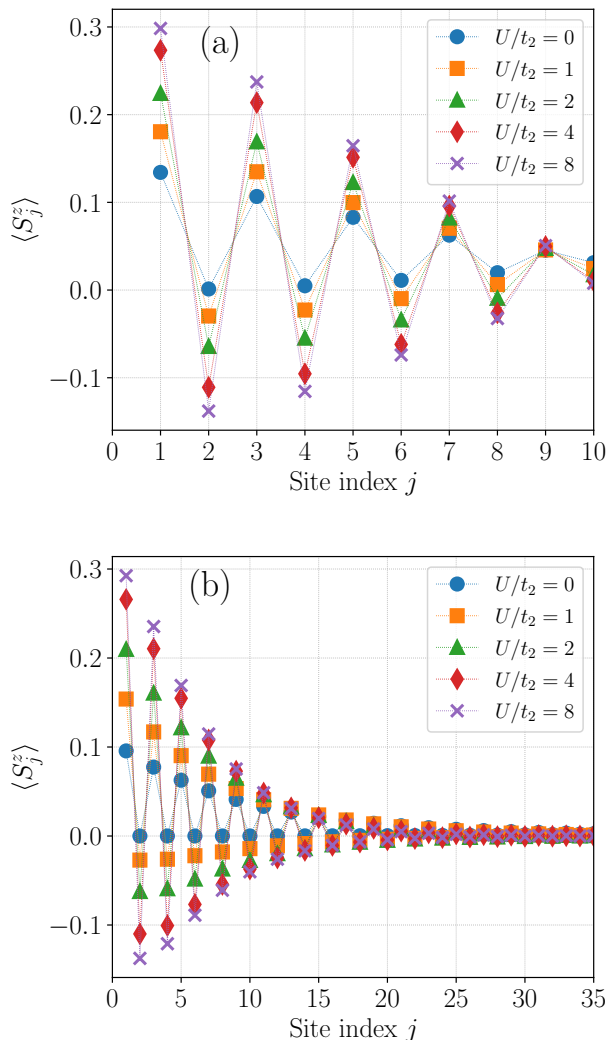


FIG. 3. (Color online) Expectation value of the spin projection for each site for a SSHC of 20 sites (panel a) and 70 sites (panel b), $S_z = 1$, $t_1 = 0.9$ and several values of U . Due to inversion symmetry with respect with the middle of the chain, only the left half is shown. The complete datasets are available in Ref. [52].

of site j are shown for the lowest state with total spin projection $S_z = 1$, and a relatively short chain ($L = 20$). For $U = 0$, the numerical values are in reasonable agreement with the analytical ones obtained from the wave functions given by Eqs. (3) and (4), although for short chains some deviations are expected. For example for the first site, the analytical result is $\langle \hat{S}_1^z \rangle = 0.108$, and the corresponding numerical result is 0.134. As U increases, the edge spin polarization grows, reaching $\langle \hat{S}_1^z \rangle = 0.298$ for $U = 8$. Instead, the neighboring even sites near the left end (and odd sites near the right end) show negligible polarization at $U = 0$, but develop finite values for $U > 0$ due to the onset of antiferromagnetic correlations. These correlations are similar to those of the Hubbard

model and arise from effective antiferromagnetic Heisenberg exchange parameters $J_1 \sim 4t_1^2/U$ and $J_2 \sim 4t_2^2/U$. In Fig. 3(b) we show similar results for a longer chain ($L = 70$). For $U = 0$, $\langle \hat{S}_j^z \rangle$ at the ends is 0.0956 compared to 0.0951 of the analytical value. In general, the magnitude of the spin projections decrease slightly with respect to the shorter chain but keeping the same qualitative behavior. For example $\langle S_{11}^z \rangle / \langle S_1^z \rangle = 0.35$ for $U = 0$ and 0.17 for $U = 8$. In the middle of the chain ($21 < j < 50$) all the values verify $|\langle S_j^z \rangle| < 0.01$.

We note that the faster decay of $\langle \hat{S}_j^z \rangle$ along the chain in Fig. 3 as U increases is consistent with the results in Fig. 2, and can be qualitatively understood as a decreasing spin end-state localization length ξ_s . While the detailed description of the evolution with U is highly non-trivial, some insight can be obtained in the strongly-interacting limit, where the interacting SSH model can be mapped onto the alternating $J_1 - J_2$ Heisenberg model [54–56]. Using the framework of field-theoretic Abelian bosonization [56], we can define the spinon velocity as $v \sim \frac{\pi}{2} \bar{J} a$, where a is the lattice parameter and $\bar{J} = (J_1 + J_2)/2$, and using the expression of the singlet-triplet bulk gap $\Delta_b \sim \bar{J} \eta^{2/3} / |\ln \eta|^{1/2}$ given in those references, where $\eta = |J_1 - J_2| / (J_1 + J_2) \approx 2\delta/t_0$ is the dimensionless alternation exchange parameter, the typical localization length of the topological end states can be estimated as $\xi_s = \hbar v / \Delta_b \sim \pi a \eta^{2/3} / |\ln \eta|^{1/2}$, which is independent of U . Indeed, in Fig. 2 the curves for $U = 4$ and $U = 8$ seem to saturate to the same value of the slope, suggesting that the strongly-interacting limit where ξ_s is constant has been reached, in accordance with the previous argument.

In Fig. 4, we compare the effective hybridization determined numerically with DMRG using Eq. (21) with our ansatz Eq. (15), using the values of the spin projections shown in Fig. 3. The agreement is remarkable. As stated in the previous Section, Eq. (21) is not expected to remain accurate when the spin distributions from the left and right overlap, an effect that occurs near the middle of the chain. This likely explains the small deviations observed close to the center of the 20-site chain. For the 70-site chain, this overlap is reduced, and the agreement between the two results holds throughout most of the system, except very near the center, even though the effective hybridization spans more than three orders of magnitude.

Having computed the spin gap and spin profile of the isolated SSHC, and having shown that the latter controls the effective hybridization, we now describe how these quantities can be extracted from STM experiments. The differential conductance at the position of the j^{th} impurity, \mathbf{r}_j , for a chain sufficiently isolated from the metallic substrate is expected to be dominated by the localized spectral density [26, 28], i.e. $dI/dV(\mathbf{r}_j, \omega) \sim \rho_j(\omega)$, where

$$\rho_j(\omega) = -\frac{1}{\pi} \text{Im} \sum_{\sigma} \langle \langle c_{j\sigma}; c_{j\sigma}^{\dagger} \rangle \rangle_{\omega}, \quad (23)$$

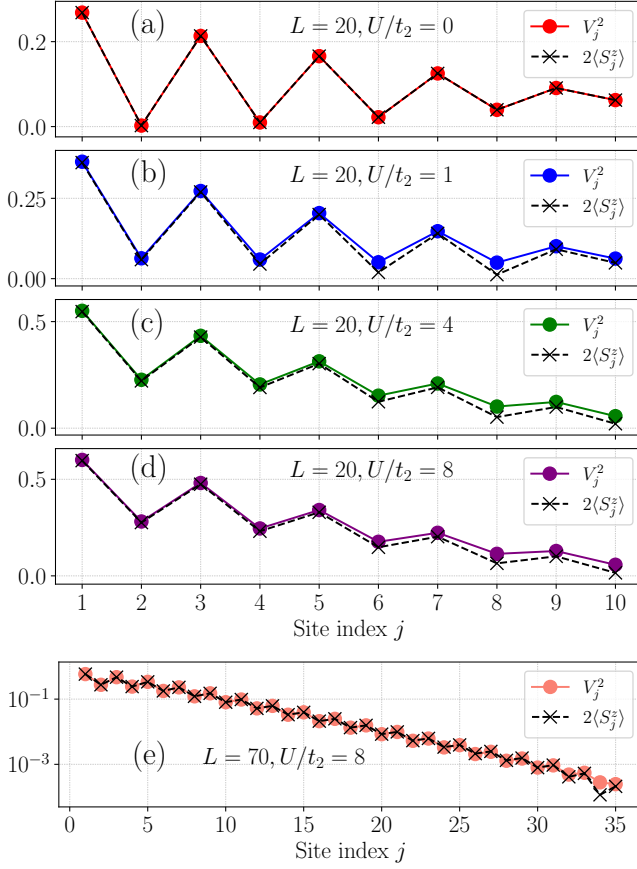


FIG. 4. (Color online) Comparison between V_j^2 calculated using Eq. (21) and $2\langle S_j^z \rangle$ obtained from Fig. 3, for various values of U/t_2 ($t_1/t_2 = 0.9$ is the same for all panels). Panels (a)-(d) correspond to a chain of 20 sites, while panel (e) (note the log scale in the vertical axis) correspond to a 70-site chain and $U/t_2 = 8$.

is the local density of states (LDOS) in the SSHC at site j , and where $\langle\langle c_{j\sigma}; c_{j\sigma}^\dagger \rangle\rangle_\omega$ is the corresponding retarded Green's function at that site. In the Kondo regime, when the conduction electrons in the STM tip effectively screen the j^{th} spin in the SSHC, the retarded Green's function can be reasonably well approximated by the expression [57, 58]

$$\langle\langle c_{j\sigma}; c_{j\sigma}^\dagger \rangle\rangle_\omega \sim \frac{Z_{K,j}}{\omega - E_F + iT_K(j)}, \quad (24)$$

where $Z_{K,j} = T_K(j)/\pi\Gamma_j$ is the quasiparticle weight, $T_K(j)$ is the position-dependent Kondo temperature given in Eq. (17), and E_F is the Fermi energy (taken as the zero of energies). In Fig. 5 we illustrate the predicted $\rho_j(\omega)$ (normalized by the LDOS at the first site at the Fermi energy), using as input the spin profile obtained in Fig. 3(a). Due to inversion symmetry, only the left half of the SSHC is shown. For illustrative purposes, we have assumed parameters $U/t_2 = 4$ and $\rho V^2/t_2 = 20$. We note that the width of the curves vary considerably

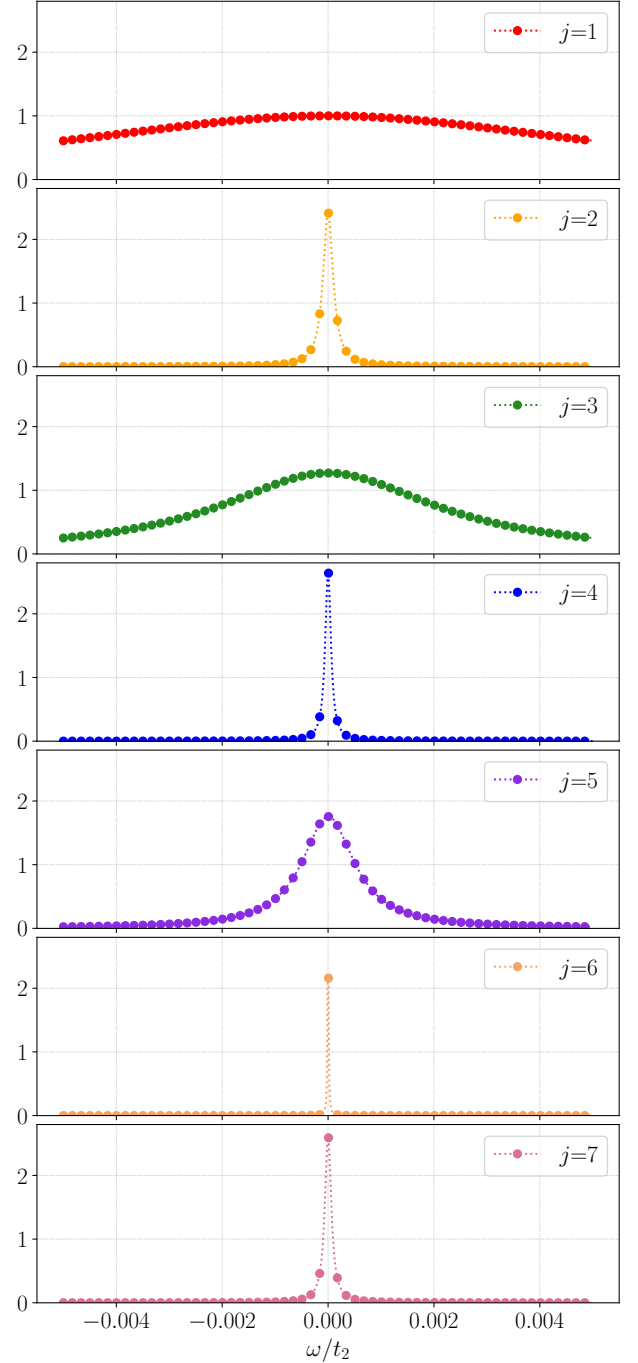


FIG. 5. (Color online) LDOS at the impurity site j normalized to the first site of the chain at $\omega = 0$, $\rho_j(\omega)/\rho_0(0)$, vs ω obtained from Eq. (23) for a chain of $L = 20$ sites. The values of V_j^2 used correspond to those used in Fig. 4(c). Other parameters are $U = 4t_2$ and $\Gamma_0 = 20t_2$ (chosen for illustrative purposes).

from site to site in the chain, indicating a strong variation of $T_K(j)$. As mentioned in the previous Section, the line shape can be altered in presence of interference effects with other orbitals [41, 42]. However in all cases,

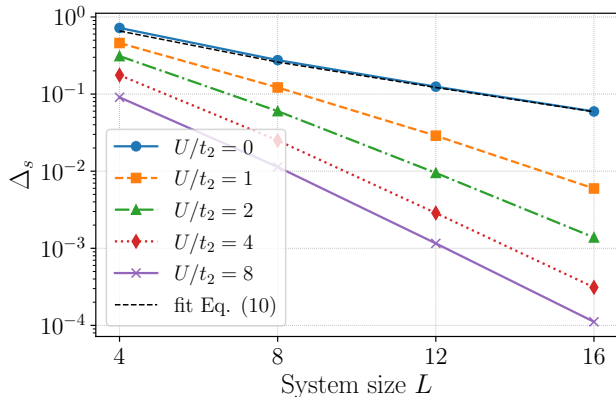


FIG. 6. (Color online) Spin gap as a function of system size for $t_1 = 0.7$ and several values of U . The dashed line for $U = 0$ corresponds to Eq. (11). Dataset available in Ref. [52].

the characteristic energy scale $T_K(j)$ can be extracted.

In the rest of this Section we discuss how the results presented above change with the difference between hoppings. From the form of the wave functions in the non-interacting case, Eqs. (3) and (4), one can define a decay length $\lambda = 1/\ln(t_2/t_1)$, which decreases with decreasing t_1 and diverges at the limit of the topological phase $t_1 \rightarrow t_2$.

In Fig. 6 we show the spin gap Δ_s for a smaller value of t_1 (0.7) as that used in Fig. 2 already shown. The same values of the interaction U are used in both figures, but smaller lengths in Fig. 6, according to the expected reduction in λ . Qualitatively, the behavior of Δ_s is similar in both figures. Again, in the non-interacting case, $U = 0$, the numerical results are in very good agreement with the analytical expression Eq. (11), but small deviations are present for the smallest sizes.

In Fig. 7, we show the expectation values $\langle \hat{S}_j^z \rangle$ as a function of the site-index j for the lowest state with total spin projection $S_z = 1$. The result is qualitatively similar to those of Figs. 3 (a) and (b). For $U = 0$, the analytical result is $\langle S_1^z \rangle = 0.256$, and the corresponding numerical result is 0.266.

VI. ZERO-FREQUENCY GREEN'S FUNCTION

The topological classification of interacting gapped phases often relies on invariants constructed from the single-particle Green's functions. These invariants capture, on equal footing, the appearance of zero-energy boundary poles—associated with genuine single-particle excitations—and of edge-localized zeros of the determinant of the Green's functions, which reflect poles of the self-energy. Several works have suggested that such zeros may correspond to neutral excitations lacking the full set of electron quantum numbers [9, 17, 18].

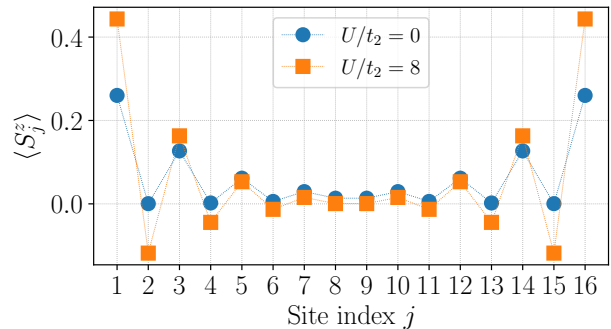


FIG. 7. (Color online) Expectation value of the spin projection for each site for a SSHC of 16 sites, $S_z = 1$, $t_1 = 0.7$ and two values of U . Dataset available in Ref. [52].

These zeros are also closely related to the topological aspects of the Luttinger theorem. Seki and Yunoki [59] have shown that the difference in the Luttinger volume of interacting and non-interacting systems is precisely given by the Luttinger integral I_L , which can take a non-trivial value when the determinant of the Green's function exhibits a zero at $\omega = 0$, in contrast to the conventional Luttinger theorem, which states that $I_L = 0$ under the assumption that perturbation theory in the interaction is valid to all orders [60, 61]. Logan and Galpin find a jump in I_L at the metal-insulator transition in the Hubbard model [62]. Moreover, non-trivial, topological values of the Luttinger integral have been shown to play an important role in impurity systems [10–13, 63, 64]. Therefore, the study of the zeros of the determinant of the Green's functions at zero energy is of fundamental interest.

In the SSH-Hubbard model considered here, it is thus natural to ask whether boundary zeros of the propagator in the topological phase can be identified with the localized free spins, which are susceptible to Kondo screening once coupled to a metallic bath. A closely related argument has been made for the half-filled Hubbard atom [14], which corresponds to the trivial edge limit of the fully dimerized ($t_1 = 0$) SSH-Hubbard chain. As we will discuss in this Section, zero eigenvalues of the propagator emerge in the thermodynamic limit of the topological phase; however, their corresponding eigenvectors are edge-localized with a characteristic length scale that differs substantially from that of the boundary spin degrees of freedom.

The properties of the Green's functions of the isolated SSH-Hubbard chain at finite U and near zero frequency can be analyzed using a combination of analytical and numerical tools. The Källén-Lehmann spectral representation of the Matsubara propagator in the zero temperature limit takes the form

$$G_{ij}(i\omega) = \sum_{\nu} \frac{D_{ij}^{\nu}}{i\omega + E_{\nu} - E_g} + \sum_{\mu} \frac{C_{ij}^{\mu}}{i\omega - E_{\mu} + E_g}, \quad (25)$$

where

$$\begin{aligned} D_{ij}^{\nu} &= \langle g | c_{j\sigma}^{\dagger} | \nu \rangle \langle \nu | c_{i\sigma} | g \rangle, \\ C_{ij}^{\mu} &= \langle g | c_{i\sigma} | \mu \rangle \langle \mu | c_{j\sigma}^{\dagger} | g \rangle. \end{aligned} \quad (26)$$

Here, $|\nu\rangle, E_{\nu}$ ($|\mu\rangle, E_{\mu}$) are eigenstates and the corresponding energies for one particle less (more) than the half-filled case and $|g\rangle$ is the ground state assumed non-degenerate. For a Kramer's degenerate ground state $|g\rangle$ is taken as a mixture of equal weight of both states.

As a consequence of the electron-hole symmetry S in the model at half filling (specifically the substitution $c_{j\sigma}^{\dagger} \rightarrow (-1)^j c_{j\sigma}$ leaves the model invariant, $SHS = H$, $Sc_{j\sigma}^{\dagger}S = (-1)^j c_{j\sigma}$), we can choose in Eq. (25) $|\mu\rangle = S|\nu\rangle$, implying $S|\mu\rangle = |\nu\rangle$) and $E_{\mu} = E_{\nu}$. Also $S|g\rangle = |g\rangle$. Then from Eq. (26)

$$C_{ij}^{\mu} = -(-1)^{j-i} \langle g | c_{i\sigma}^{\dagger} | \nu \rangle \langle \nu | c_{j\sigma} | g \rangle = -(-1)^{j-i} D_{ji}^{\nu}. \quad (27)$$

We note that because of the presence of a charge gap at finite U , there are no poles at zero frequency, and therefore one can safely evaluate $\omega = 0$ in Eq. (25). Using Eq. (27), we obtain

$$G_{ij}(0) = \sum_{\nu} \frac{D_{ij}^{\nu} - (-1)^{j-i} D_{ji}^{\nu}}{E_{\nu} - E_g}. \quad (28)$$

Clearly, from Eq. (28),

$$G_{ji}(0) = -(-1)^{j-i} G_{ij}(0). \quad (29)$$

For a system with time-reversal symmetry and without spin-orbit coupling one expects the Lehmann amplitudes in Eq. (26) to be real. Together with Eq. (29), this implies that the zero-frequency Green's function matrix $G(0)$, with elements $G_{ij}(0)$, is real, symmetric, and vanishes for even $j - i$, consistent with chiral sublattice symmetry. A more stringent result was recently reported in Ref. [65] for the large- U limit, where $G(0)$ acquires a tridiagonal structure, coupling only nearest-neighbor sites. Quite generally, the resulting structure of $G(0)$ is that of an effective noninteracting tight-binding model with electron-hole symmetry S . Consequently, each positive eigenvalue has a corresponding negative partner. For a chain with an odd number of sites, this symmetry enforces the presence of a zero eigenvalue, independently of the ratio t_1/t_2 . For a chain with an even number

of sites, two eigenvalues approach zero in the thermodynamic limit of the topological phase ($t_1 < t_2$). This is consistent with the numerical evaluation of the bulk topological invariant reported by Manmana *et al.* [7].

To verify the predictions of the symmetry analysis above, we performed a numerical check of the Green's function matrix for a small chain of seven sites with $U = 1$, $t_2 = 1$, and several small t_1 values. For each of the two degenerate $S_z = \pm 1/2$ ground states we constructed the corresponding propagators and then averaged them. In the spin-polarized cases, sizable matrix elements connect sites within the same sublattice, but these vanish upon averaging, in agreement with the symmetry considerations above. For small t_1 , we find that the off-diagonal element $G_{12}(0)$ scales as $\sim t_1^3$, consistent with perturbative arguments. Consequently, the zero-eigenvector of the propagator—the “dark orbital”—is strongly localized at the first site, in sharp contrast with the boundary spin distribution, which, as shown in Figs. 3 and 7, extends with appreciable weight to the third site and scales as $\sim t_1^2$. We further note that breaking electron-hole symmetry, for instance by shifting the on-site energy, displaces the zeros of the Green's function away from $\omega = 0$ (see Supplemental Material of Ref. [9]), while leaving the localized end spins unaffected.

It is interesting to analyze the contribution of the states near the Fermi energy for the non-interacting case. Using the results of Section III we obtain for odd j

$$G_{jj}(\omega) = \frac{z^{j-1}(1-z^2)}{2(1-z^L)} \left(\frac{1}{\omega + t_{LR}} + \frac{1}{\omega - t_{LR}} \right). \quad (30)$$

For an infinite chain $t_{LR} \rightarrow 0$, and the Green functions have a pole at $\omega = 0$. For a finite chain, the pole is converted into a zero. However, this zero does not imply a vanishing of the determinant of one-particle Green functions, which is the quantity related with topology [6, 7, 9].

In addition, because of the wavefunction decay factor z^{j-1} [see Eq. (5)], the low-energy features are substantially more marked at the end of the chain, where also larger expectation values of the spin projection are present.

VII. SUMMARY AND DISCUSSION

In this work we provide a theoretical framework for probing the spins localized near the ends of an interacting Su-Schrieffer-Heeger chain in the topological phase, using scanning tunneling microscopy in the contact regime, combined with electron spin resonance in the tunneling regime.

We propose that when the STM tip couples directly to these localized spins, the system maps onto an effective Anderson impurity model, producing a Kondo resonance whose spatially dependent width encodes the spin profile of the end states.

While for a non-interacting infinite open chain vanishingly small charge and spin excitation gaps occur in the lowest-energy subspace due to the presence of zero-energy states localized at the ends, in the interacting case a finite charge gap opens (albeit with a vanishingly small spin gap) in the infinite open chain. In other words the electronic zero-energy excitations (with charge and spin) in the non-interacting case $U = 0$ disappear for finite U despite the fact that zero-energy spin excitations remain in the infinite chain. For finite chains the end states interact leading to a finite spin gap which, as we have described, can be measured combining STM and ESR.

Using density-matrix renormalization group, we compute the spin gap and spin polarization for chains of different lengths and interaction strengths, showing how correlations reduce the spin gap and enhance spin localization at the edges. For $U = 0$ we obtain analytical results for the spin gap and distribution of the spin projection $\langle S_j^z \rangle$ along an open topological SSHC which agree well with DMRG results for sufficiently long chains. In the interacting case, the magnitude of the spin projection and its dependence on position become evident in the numerical calculations choosing the subspace with total spin projection $S_z = 1$. The numerical results for these two quantities and its dependence on parameters clarify the nature of the spins at the end states and might serve as a guide for future research.

As a consistency check with previous works defining topology via single-particle Green's function invariants,

we verified that the zero-frequency propagator respects chiral sublattice symmetry, which enforces the presence of zero eigenvalues in the topological regime. We numerically analyzed the corresponding eigenvectors, finding them strongly localized at the chain ends, in contrast with the more extended distribution of the boundary spins.

Taken together, our results establish STM and ESR as powerful probes of correlated topological boundary excitations, providing a promising route to characterize boundary spins in interacting SSH chains.

Our proposal might be useful to detect magnetic impurities in Heisenberg chains [66]. It would also be interesting to extend our theory to systems which have fractional spin end modes, like the XXZ spin-1/2 model [67, 68] and time-reversal invariant topological superconductors [38, 69, 70].

ACKNOWLEDGMENTS

We thank Pablo Cornaglia for useful discussions. L.P.G. acknowledges support provided by the FRS-FNRS Belgium and the L'Oréal-UNESCO for Women in Science Programme. The results presented in this work have been obtained by using the facilities of the CCT-Rosario Computational Center, member of the High Performance Computing National System (SNCAD, Mincyt-Argentina).

-
- [1] Y. Ando, Topological insulator materials, *Journal of the Physical Society of Japan* **82**, 102001 (2013).
 - [2] W. P. Su, J. R. Schrieffer, and A. J. Heeger, Solitons in polyacetylene, *Phys. Rev. Lett.* **42**, 1698 (1979).
 - [3] J. Zak, Berry's phase for energy bands in solids, *Phys. Rev. Lett.* **62**, 2747 (1989).
 - [4] J. K. Asbóth, L. Oroszlány, and A. Pályi, *A Short Course on Topological Insulators* (Springer International Publishing, 2016).
 - [5] A. A. Aligia, Topological invariants based on generalized position operators and application to the interacting Rice-Mele model, *Phys. Rev. B* **107**, 075153 (2023).
 - [6] V. Gurarie, Single-particle Green's functions and interacting topological insulators, *Phys. Rev. B* **83**, 085426 (2011).
 - [7] S. R. Manmana, A. M. Essin, R. M. Noack, and V. Gurarie, Topological invariants and interacting one-dimensional fermionic systems, *Phys. Rev. B* **86**, 205119 (2012).
 - [8] T. Yoshida, R. Peters, S. Fujimoto, and N. Kawakami, Characterization of a Topological Mott Insulator in One Dimension, *Phys. Rev. Lett.* **112**, 196404 (2014).
 - [9] N. Wagner, L. Crippa, A. Amaricci, P. Hansmann, M. Klett, E. J. König, T. Schäfer, D. D. Sante, J. Cano, A. J. Millis, A. Georges, and G. Sangiovanni, Mott insulators with boundary zeros, *Nature Communications* **14**, 7531 (2023).
 - [10] R. Žitko, G. G. Blesio, L. O. Manuel, and A. A. Aligia, Iron phthalocyanine on Au(111) is a "non-Landau" Fermi liquid, *Nature Communications* **12**, 6027 (2021).
 - [11] G. G. Blesio, R. Žitko, L. O. Manuel, and A. A. Aligia, Topological quantum phase transition of nickelocene on Cu(100), *SciPost Phys.* **14**, 042 (2023).
 - [12] G. G. Blesio and A. A. Aligia, Topological quantum phase transition in individual Fe atoms on MoS₂/Au(111), *Phys. Rev. B* **108**, 045113 (2023).
 - [13] G. G. Blesio, L. O. Manuel, and A. A. Aligia, Anisotropy-driven topological quantum phase transition in magnetic impurities, *Materials for Quantum Technology* **4**, 042001 (2024).
 - [14] A. Blason and M. Fabrizio, Unified role of Green's function poles and zeros in correlated topological insulators, *Phys. Rev. B* **108**, 125115 (2023).
 - [15] L. Peralta Gavensky, S. Sachdev, and N. Goldman, Connecting the Many-Body Chern Number to Luttinger's Theorem through Středa's Formula, *Phys. Rev. Lett.* **131**, 236601 (2023).
 - [16] N. Wagner, D. Guerci, A. J. Millis, and G. Sangiovanni, Edge Zeros and Boundary Spinons in Topological Mott Insulators, *Phys. Rev. Lett.* **133**, 126504 (2024).
 - [17] M. Fabrizio, Spin-Liquid Insulators Can Be Landau's Fermi Liquids, *Phys. Rev. Lett.* **130**, 156702 (2023).
 - [18] E. Pangburn, C. Pépin, and A. Banerjee, Topological charge excitations and Green's function zeros in paramagnetic Mott insulators, *Phys. Rev. B* **112**, 085105 (2025).

- (2025).
- [19] R. Flores-Calderón and C. Hooley, Weyl-Mott point: Topological and non-Fermi liquid behavior from an isolated Green's function zero, *Phys. Rev. B* **111**, 235139 (2025).
- [20] S. Mishra, G. Catarina, F. Wu, R. Ortiz, D. Jacob, K. Eimre, J. Ma, C. A. Pignedoli, X. Feng, P. Ruffieux, J. Fernández-Rossier, and R. Fasel, Observation of fractional edge excitations in nanographene spin chains, *Nature* **598**, 287 (2021).
- [21] C. Zhao, G. Catarina, J.-J. Zhang, J. C. G. Henriques, L. Yang, J. Ma, X. Feng, O. Gröning, P. Ruffieux, J. Fernández-Rossier, and R. Fasel, Tunable topological phases in nanographene-based spin-1/2 alternating-exchange Heisenberg chains, *Nature Nanotechnology* **19**, 1789 (2024).
- [22] L. Edens, F. R. Lara, T. Sai, K. Biswas, M. Vilas-Varela, F. Schulz, D. Peña, and J. I. Pascual, Spin and charge control of topological end states in chiral graphene nanoribbons on a 2d ferromagnet (2025), [arXiv:2505.23468 \[cond-mat.mes-hall\]](https://arxiv.org/abs/2505.23468).
- [23] H. Wang, P. Fan, J. Chen, L. Jiang, H.-J. Gao, J. L. Lado, and K. Yang, Construction of topological quantum magnets from atomic spins on surfaces, *Nature Nanotechnology* **19**, 1782 (2024).
- [24] A. Maiellaro, H. Aubin, A. Mesáros, and P. Simon, Local dynamics and detection of topology in spin-1 chains, *Phys. Rev. B* **110**, L220410 (2024).
- [25] M. Ormaza, P. Abufager, B. Verlhac, N. Bachellier, M.-L. Bocquet, N. Lorente, and L. Limot, Controlled spin switching in a metallocene molecular junction, *Nature Communications* **8**, 1974 (2017).
- [26] M. Mohr, M. Gruber, A. Weismann, D. Jacob, P. Abufager, N. Lorente, and R. Berndt, Spin dependent transmission of nickelocene-Cu contacts probed with shot noise, *Phys. Rev. B* **101**, 075414 (2020).
- [27] M. Kögler, N. Néel, L. Limot, and J. Kröger, Structural Manipulation of Spin Excitations in a Molecular Junction, *Nano Letters* **24**, 14355 (2024).
- [28] D.-J. Choi, P. Abufager, L. Limot, and N. Lorente, From tunneling to contact in a magnetic atom: The non-equilibrium Kondo effect, *The Journal of Chemical Physics* **146**, 092309 (2016).
- [29] K. Yang, P. Willke, Y. Bae, A. Ferrón, J. L. Lado, A. Ardavan, J. Fernández-Rossier, A. J. Heinrich, and C. P. Lutz, Electrically controlled nuclear polarization of individual atoms, *Nature Nanotechnology* **13**, 1120 (2018).
- [30] P. Willke, Y. Bae, K. Yang, J. L. Lado, A. Ferrón, T. Choi, A. Ardavan, J. Fernández-Rossier, A. J. Heinrich, and C. P. Lutz, Hyperfine interaction of individual atoms on a surface, *Science* **362**, 336 (2018).
- [31] X. Zhang, C. Wolf, Y. Wang, H. Aubin, T. Bilgeri, P. Willke, A. J. Heinrich, and T. Choi, Electron spin resonance of single iron phthalocyanine molecules and role of their non-localized spins in magnetic interactions, *Nature Chemistry* **14**, 59 (2022).
- [32] Q. Chen, H. Du, X. Meng, J. Wang, J. Liao, B. Li, W. Hu, Q. Fan, S. Tan, C. Ma, J. Yang, J. G. Hou, and B. Wang, Microscopic Mechanism of Coexisting Electron Spin Resonance and Kondo Resonance in a Single Iron Phthalocyanine Molecule, *Phys. Rev. Lett.* **135**, 086403 (2025).
- [33] Y. del Castillo and J. Fernández-Rossier, Probing spin fractionalization with electron spin resonance based on scanning tunneling microscopy, *Phys. Rev. B* **110**, 045145 (2024).
- [34] Y.-C. Tzeng, L. Dai, M.-C. Chung, L. Amico, and L.-C. Kwek, Entanglement convertibility by sweeping through the quantum phases of the alternating bonds XXZ chain, *Scientific Reports* **6**, 10.1038/srep26453 (2016).
- [35] B. F. Márquez, N. Aucar Boidi, K. Hallberg, and A. A. Aligia, Phase diagram and topology of the xxz chain with alternating bonds and staggered magnetic field, *Phys. Rev. B* **109**, 235143 (2024).
- [36] A. Alase, E. Cobanera, G. Ortiz, and L. Viola, Exact solution of quadratic fermionic hamiltonians for arbitrary boundary conditions, *Phys. Rev. Lett.* **117**, 076804 (2016).
- [37] A. Alase, E. Cobanera, G. Ortiz, and L. Viola, Generalization of Bloch's theorem for arbitrary boundary conditions: Theory, *Phys. Rev. B* **96**, 195133 (2017).
- [38] A. A. Aligia and L. Arrachea, Entangled end states with fractionalized spin projection in a time-reversal-invariant topological superconducting wire, *Phys. Rev. B* **98**, 174507 (2018).
- [39] P. W. Anderson, A poor man's derivation of scaling laws for the Kondo problem, *Journal of Physics C: Solid State Physics* **3**, 2436 (1970).
- [40] F. D. M. Haldane, Scaling theory of the asymmetric anderson model, *Phys. Rev. Lett.* **40**, 416 (1978).
- [41] O. Újsághy, J. Kroha, L. Szunyogh, and A. Zawadowski, Theory of the fano resonance in the stm tunneling density of states due to a single kondo impurity, *Phys. Rev. Lett.* **85**, 2557 (2000).
- [42] J. Fernández, P. Roura-Bas, and A. A. Aligia, Theory of differential conductance of co on cu(111) including co *s* and *d* orbitals, and surface and bulk cu states, *Phys. Rev. Lett.* **126**, 046801 (2021).
- [43] J. R. Schrieffer and P. A. Wolff, Relation between the anderson and kondo hamiltonians, *Phys. Rev.* **149**, 491 (1966).
- [44] P. S. Cornaglia and D. R. Grempel, Strongly correlated regimes in a double quantum dot device, *Phys. Rev. B* **71**, 075305 (2005).
- [45] L. G. G. V. Dias da Silva, N. P. Sandler, K. Ingersent, and S. E. Ulloa, Zero-Field Kondo Splitting and Quantum-Critical Transition in Double Quantum Dots, *Phys. Rev. Lett.* **97**, 096603 (2006).
- [46] L. Vaugier, A. A. Aligia, and A. M. Lobos, Comment on "Zero-field Kondo Splitting and Quantum-Critical Transition in Double Quantum Dots", *Phys. Rev. Lett.* **99**, 209701 (2007).
- [47] L. G. G. V. Dias da Silva, N. P. Sandler, K. Ingersent, and S. E. Ulloa, Dias da Silva et al. Reply., *Phys. Rev. Lett.* **99**, 209702 (2007).
- [48] L. Vaugier, A. A. Aligia, and A. M. Lobos, Spectral density of an interacting dot coupled indirectly to conducting leads, *Phys. Rev. B* **76**, 165112 (2007).
- [49] P. A. Almeida, E. Vernek, E. V. Anda, S. E. Ulloa, and G. B. Martins, Identifying an effective model for the two-stage Kondo regime: Numerical renormalization group results, *Phys. Rev. B* **111**, 085146 (2025).
- [50] Z.-H. Yuan, G. Gong, T. Jing, H. Shang, S. Jin, D. Yuan, W. Zhou, and Y.-C. Xiong, Gate-controlled two-stage Kondo effect in a metal-free polycyclic aromatic hydrocarbon diradical molecular switch: A DFT+NRG insight, *The Journal of Chemical Physics* **163**, 114304 (2025).

- [51] H. Huang, R. Drost, J. Senkpiel, C. Padurariu, B. Kubala, A. L. Yeyati, J. C. Cuevas, J. Ankerhold, K. Kern, and C. R. Ast, Quantum phase transitions and the role of impurity-substrate hybridization in Yu-Shiba-Rusinov states, *Communications Physics* **3**, 199 (2020).
- [52] A. A. Aligia, A. M. Lobos, L. Peralta Gavensky, and C. J. Gazza, *Probing Boundary Spins in the Su-Schrieffer-Heeger-Hubbard model: datasets* (2025).
- [53] M. Fishman, S. R. White, and E. M. Stoudenmire, The ITensor Software Library for Tensor Network Calculations, *SciPost Phys. Codebases*, 4 (2022).
- [54] K. Hida, Crossover between the Haldane-gap phase and the dimer phase in the spin-1/2 alternating Heisenberg chain, *Phys. Rev. B* **45**, 2207 (1992).
- [55] M. C. Cross and D. S. Fisher, A new theory of the spin-Peierls transition with special relevance to the experiments on TTFCuBDT, *Phys. Rev. B* **19**, 402 (1979).
- [56] E. Orignac, Quantitative expression of the spin gap via bosonization for a dimerized spin-1/2 chain, *The European Physical Journal B - Condensed Matter and Complex Systems* **39**, 335 (2004).
- [57] A. C. Hewson, *The Kondo Problem to Heavy Fermions* (Cambridge University Press, Cambridge, 1993).
- [58] O. Agam and A. Schiller, Projecting the Kondo Effect: Theory of the Quantum Mirage, *Phys. Rev. Lett.* **86**, 484 (2001).
- [59] K. Seki and S. Yunoki, Topological interpretation of the Luttinger theorem, *Phys. Rev. B* **96**, 085124 (2017).
- [60] J. M. Luttinger, Fermi surface and some simple equilibrium properties of a system of interacting fermions, *Phys. Rev.* **119**, 1153 (1960).
- [61] J. M. Luttinger and J. C. Ward, Ground-State Energy of a Many-Fermion System. II, *Phys. Rev.* **118**, 1417 (1960).
- [62] D. E. Logan and M. R. Galpin, Mott insulators and the doping-induced Mott transition within DMFT: exact results for the one-band Hubbard model, *Journal of Physics: Condensed Matter* **28**, 025601 (2015).
- [63] O. J. Curtin, Y. Nishikawa, A. C. Hewson, and D. J. G. Crow, Fermi Liquids and the Luttinger Integral, *Journal of Physics Communications* **2**, 031001 (2018).
- [64] G. G. Blesio, L. O. Manuel, P. Roura-Bas, and A. A. Aligia, Topological quantum phase transition between Fermi liquid phases in an Anderson impurity model, *Phys. Rev. B* **98**, 195435 (2018).
- [65] C. Lehmann, L. Crippa, G. Sangiovanni, and J. C. Budich, Probing Green's Function Zeros by Cotunneling through Mott Insulators, *Phys. Rev. Lett.* **135**, 106303 (2025).
- [66] S. Eggert and I. Affleck, Magnetic impurities in half-integer-spin Heisenberg antiferromagnetic chains, *Phys. Rev. B* **46**, 10866 (1992).
- [67] P. Kattel, P. R. Pasnoori, J. H. Pixley, and N. Andrei, Edge modes and boundary impurities in the anisotropic Heisenberg spin chain, *Phys. Rev. B* **111**, 174430 (2025).
- [68] P. Kattel, Y. Tang, J. H. Pixley, and N. Andrei, Edge spin fractionalization in open one-dimensional spin- s quantum antiferromagnets, *Phys. Rev. B* **111**, L220402 (2025).
- [69] A. Keselman, L. Fu, A. Stern, and E. Berg, Inducing time-reversal-invariant topological superconductivity and fermion parity pumping in quantum wires, *Phys. Rev. Lett.* **111**, 116402 (2013).
- [70] A. A. Aligia and A. Camjayi, Exact analytical solution of a time-reversal-invariant topological superconducting wire, *Phys. Rev. B* **100**, 115413 (2019).